Determining dominant driving forces affecting controlled protein release from polymeric nanoparticles

Josh Smith,[a] Kayla G. Sprenger,[a] Rick Liao, Andrea Joseph, Elizabeth Nance,[b] and Jim Pfaendtner[b]
Department of Chemical Engineering, University of Washington, 105 Benson Hall, 3781 Okanogan Lane NE, Seattle, Washington 98195

(Received 9 March 2017; accepted 26 April 2017; published 19 May 2017)

Enzymes play a critical role in many applications in biology and medicine as potential therapeutics. One specific area of interest is enzyme encapsulation in polymer nanostructures, which have applications in drug delivery and catalysis. A detailed understanding of the mechanisms governing protein/polymer interactions is crucial for optimizing the performance of these complex systems for different applications. Using a combined computational and experimental approach, this study aims to quantify the relative importance of molecular and mesoscale driving forces to protein release from polymeric nanoparticles. Classical molecular dynamics (MD) simulations have been performed on bovine serum albumin (BSA) in aqueous solutions with oligomeric surrogates of poly(lactic-*co*-glycolic acid) copolymer, poly(styrene)-poly(lactic acid) copolymer, and poly(lactic acid). The simulated strength and location of polymer surrogate binding to the surface of BSA have been compared to experimental BSA release rates from nanoparticles formulated with these same polymers. Results indicate that the self-interaction tendencies of the polymer surrogates and other macroscale properties may play governing roles in protein release. Additional MD simulations of BSA in solution with poly(styrene)-acrylate copolymer reveal the possibility of enhanced control over the enzyme encapsulation process by tuning polymer self-interaction. Last, the authors find consistent protein surface binding preferences across simulations performed with polymer surrogates of varying lengths, demonstrating that protein/polymer interactions can be understood in part by studying the interactions and affinity of proteins with small polymer surrogates in solution. [http://dx.doi.org/10.1116/1.4983154]

I. INTRODUCTION

In recent years, proteins have played an increasingly important role as catalysts in the fields of biology and medicine, wherein protein delivery is of interest for therapeutic intervention in many diseases.[1] However, avoiding stability and activity loss of the protein in biological environments remains an active area of research. Several platforms have emerged around the concept of protein immobilization within a material to stabilize the proteins while still allowing for substrate diffusion to the protein through the pores of the material. Polymer nanoparticles (NPs) are particularly promising delivery vehicles for encapsulated proteins due to their high protein-loading capacity and porous nanostructure.[2,3] These properties are especially important for medical applications because delivering high drug payloads to sites of interest by polymer nanocarriers can reduce toxicity and off-site side effects. Additionally, therapeutic effects can only be achieved if the proteins are delivered in a stable and active form. Polymer NPs can promote stability through physical confinement of the protein and enable increased activity by serving as a *p*H buffer that provides proteins with an ideal chemical environment.[4,5]

Recent applications of protein-encapsulated polymer nanostructures include proteins in polymer nanoshells[6] or in polymer microspheres[7] for controlled drug release, leading to increases in protein activity and stability in both cases. In the latter study, protein stability was further increased with the addition of stabilizers like polyethylene glycol (PEG) to the polymer microspheres. Many variable protein/polymer frameworks exist due to the numerous factors that can influence the effect of encapsulation on the protein's stability and activity, which include: the nature of the protein/carrier interaction, the protein's ability to undergo conformational change within the carrier, the protein's surrounding microenvironment, the chemical and physical properties of the carrier, the properties of the protein/polymer linker, and the immobilization conditions of the experiments. The underlying mechanisms governing many of these relationships are still unknown, and thus optimization of the performance of these protein/polymer structures is carried out through an exhaustive and experimental trial-and-error process.

Physics-based computational methods could provide needed fundamental insight into the interactions of proteins and polymers. Additionally, simulations could be used as a preliminary tool to parse the vast parameter design space of polymer nanostructures to determine optimal protein/polymer test candidates for given applications, thus providing a powerful guide for experiments. Despite this immense

[a]J. Smith and K. G. Sprenger contributed equally to this work.
[b]Authors to whom correspondence should be addressed; electronic addresses: eanance@uw.edu; jpfaendt@uw.edu

potential, the use of molecular simulations to study drug/polymer interactions has been limited by the computational expense of simulating these large-scale systems (i.e., proteins and lengthy polymer chains together),[8,9] which is exacerbated by the long relaxation times of these systems. To this end, computational studies to date have taken the approach of simulating the interactions of single or multiple drug molecules with a finite and relatively limited number of solvated polymer chains.[10,11] Another approach includes the use of coarse-grained models like dissipative particle dynamics to study larger polymer-based systems.[12–14] However, this approach sacrifices atomistic detail that is necessary to fully understand protein/polymer interactions and to be able to predict or fine-tune these interactions for new applications. Additionally, these methods are limited in their ability to quantitatively compare against experimental observations such as drug release kinetics. The need persists for a fundamental understanding of the major determinants of protein release and retention from synthetic biomaterials.

Herein, we use a combined experimental and computational approach to probe the relative contributions of various physical phenomena in determining protein release from polymeric nanoparticles. Experimental techniques—better suited to explore macroscopic phenomena such as transport effects and polymer matrix properties—are used to measure release profiles for model protein bovine serum albumin (BSA) from NPs that span a range of chemistries and sizes. These include poly(lactic-*co*-glycolic acid) (PLGA) copolymer, poly(styrene)-poly(lactic acid) (PS-PLA) copolymer, and poly(lactic acid) (PLA), from ∼85 to 160 nm in diameter in NP form. Results rule out transport effects as a determining factor in release time, suggesting the need for computational study of nanoscale physical interactions. We have used classical, fully atomistic molecular dynamics (MD) simulations to investigate the relative importance of polymer–protein and polymer–polymer interactions as the basis for a predictive framework to design protein encapsulation systems for medical applications. Studies are performed on BSA exposed to aqueous solutions of trimeric PLGA, PLA, and PS-PLA. Additional simulations were performed with trimers of polystyrene (PS) as a control. Analysis of amino acid preferences and spatial distribution of polymer binding on the BSA surface suggest insufficient differentiation between PLA and PLGA to explain their different BSA release profiles. The aggregation tendency of PS in simulations with PS-PLA or PS alone supports the hypothesis from experiment that PS-PLA core–shell arrangement is responsible for similar release from PLA and PS-PLA NPs. Taken together, the combined study suggests that polymer matrix properties that tend toward self-interaction may outweigh polymer–protein interactions for controlled protein release. Simulations are extended to study trimers of poly(styrene)-acrylate (PSAC) copolymer, which may be tuned for the relative strength of self-interactions and protein interactions, providing a handle for future experimental optimization.

II. EXPERIMENTAL METHODS

A. Materials

BSA conjugated with fluoro-isothiocyanate (BSA-FITC, or BSA) was purchased from Sigma Aldrich. PLGA copolymer (50%/50% molar ratio), PS-PLA copolymer (25%/75% molar ratio), and PLA were purchased from PolySciTech Akina, Inc. Poly(vinyl alcohol) (PVA) and bile salts (cholic acid, CHA), were obtained from Sigma Aldrich. Dulbecco's phosphate buffered saline (PBS) was obtained from Corning. Dichloromethane (DCM) was obtained from Fisher Chemical.

B. Nanoparticle formulation

For polymer NP formulations, $w_1/o/w_2$ (water/oil/water) double emulsions were used, adapted from previously published protocols.[15] Polymer of 50 mg was dissolved in 1 ml DCM and added to 0.2 ml deionized (DI) water containing 5 mg dissolved BSA and 0.5 wt. % PVA. The solution was immediately sonicated, with 1 s:1 s on/off for 2 min. The first emulsion was then added to 4 ml water with 2% PVA, and immediately sonicated, following 1 s:1 s on/off sonication for 2 min. For PLA and PLGA NP formulations, the first emulsion was performed at 30% amplitude, and the second emulsion at 20% amplitude using an ultrasonic processor (QSonics). For PS-PLA NP formulations, the first and second emulsion amplitudes used were 40% and 30%, respectively. Immediately after the second emulsion, the sample was added to 25 ml of water containing 1% PVA and either 1% CHA for PLA and PS-PLA formulations, or 1× PBS for PLGA formulations. After 3 h of stirred incubation to evaporate off DCM, particles were collected via ultracentrifugation at 2000 relative centrifugal units (RCF) for 2 min to remove any large aggregates or undissolved polymer. Particles were then collected at 100 000 RCF for 60 min. The particles were then washed once with DI water in a 25-min centrifugation at 100 000 RCF prior to resuspension in 1 ml 1× PBS. For PS-PLA particles, the wash step was eliminated to avoid potential aggregation.

C. Nanoparticle characterization

NP hydrodynamic diameter (size), polydispersity index (PDI), and zeta potential (ZP) were measured using dynamic light scattering (Malvern Zetasizer). Encapsulation efficiency (EE) was quantified using ultraviolet-visible light spectrometry (UV-Vis) compared to a standard calibration curve for BSA-FITC dissolved in 1× PBS. EE is defined as follows:

$$\%\mathrm{EE} = \frac{\text{weight of drug encapsulated in NP}}{\text{total weight of drug added into formulation}} \times 100\%. \quad (1)$$

D. BSA release

BSA-FITC release studies were performed for all NP formulations by reconstituting and incubating NPs in 10 ml 1×

PBS on a stir plate at 37 °C. At specified time points, NPs were centrifuged at 100 000 RCF for 25 min, and the supernatant was collected. The amount of BSA in the supernatant at the time points of 1, 2 4, 8 h, and 1, 2, 3, 4, 5, 6, and 7 days was analyzed using UV-Vis, as described above. % BSA release was calculated by dividing the concentration of BSA in the supernatant by the total initial encapsulated amount.

III. COMPUTATIONAL METHODS

Representative structures of all polymer surrogates and BSA are shown in Fig. 1, with the addition of PS as a control. Additional simulations of other protein/polymer surrogate systems are described in Sec. IV. BSA was solvated in 2 wt. % of the polymer surrogates in water. Solutions with PLGA were simulated as trimers of alternating lactic acid (LA) and glycolic acid (GA) monomers (six units total per molecule) to mimic experimental conditions of a PLGA random copolymer with an approximately 50%/50% molar ratio of LA and GA. Solutions with PS-PLA were simulated as individual trimers of PS and PLA in an approximately 25%/75% molar ratio (three monomers per molecule of either PS or PLA; 2 wt. % total surrogate) to match experimental conditions of the diblock copolymer. Packmol[16] was used to generate cubic boxes of the protein/ionic liquid systems, resulting in approximately 120 000 particles per system. A single trial was conducted for each system. The low polymer wt. % in our solutions was motivated by the hypothesis that protein surface binding properties can be more accurately studied at low solute concentrations due to minimization of random surface collisions.

Polymer surrogates were parameterized with the general Amber force field,[17] with atomic charges obtained via

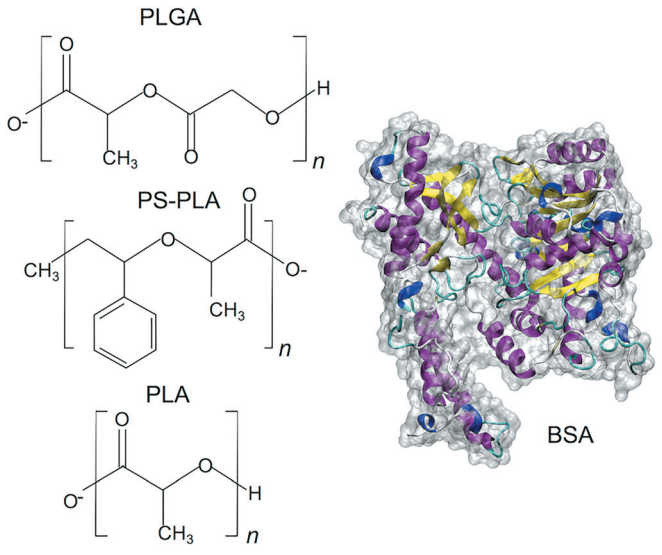

FIG. 1. Protein and surrogates used to model polymer nanoparticles in MD simulations. Surrogates include trimers of PLGA, PS-PLA, and PLA. Purple, blue, yellow, cyan, and white coloring indicate an α-helix, α_{310}-helix, β-sheet, turn, and random coil, respectively, and the protein (BSA) is also shown in surface representation in gray.

Gaussian[18] and the restrained electrostatic potential[19] partial charge calculation method. Trimer charges were adjusted to more closely match monomer charge distributions (Sec. IV F). The Amber14SB (Ref. 20) and TIP3P (Ref. 21) force fields were used to model the protein and water, respectively, and topology for the polymer surrogates was built to mimic the intracellular *p*H of the brain that is maintained at approximately 7.2.[22] We are particularly interested in better understanding protein/polymer interactions in therapeutic NPs for delivery to the brain due to the growing body of literature demonstrating the impact polymer NP properties have on determining site specific delivery for brain diseases.[23–26] Simulations were carried out with the GROMACS 5.1.2 (Ref. 27) MD engine, using a time step of 2 fs and full periodic boundary conditions. For all MD simulations, the LINCS algorithm[28] was employed to constrain bonds between hydrogen and heavy atoms, and particle mesh Ewald summations[29] were used to calculate long-range electrostatic interactions between the particles with a cutoff value of 10 Å. van der Waals forces were also calculated with a cutoff value of 10 Å and shifted to zero, and neighbor lists were updated every ten steps with a cutoff of 10 Å.

Following a steepest descent energy minimization of the initial configurations of each system for 40 000 steps, a short 200 ps simulation in the isothermal-isobaric (NPT) ensemble was run to equilibrate the systems at 298.15 K and 1 bar, with the Bussi-Donadio-Parrinello thermostat[30] and Berendsen barostat.[31] It is well known that the Berendsen barostat is useful for quickly equilibrating the box size to the correct average pressure, but the fluctuations from the Berendsen barostat do not correctly resemble the NPT ensemble. Therefore, as is custom in the field, we used the Parrinello-Rahman barostat[32] for the production runs, with the same thermostat. Simulations were run for 200 ns, unless otherwise indicated. In solutions containing the highly hydrophobic PS surrogate (i.e., with either PS or PS-PLA), additional 50 ns simulations were run with the PLUMED 2.0 plugin[33] to prevent PS aggregation (see Sec. IV A). Enforcing a maximum number of contacts allowed between each PS atom and all other PS atoms in the system prevented aggregation. The maximum number of contacts was set equal to the original number observed in the fully dispersed systems obtained from Packmol. Contacts were defined via a simple switching function that ranged from 0 to 1 with a reference bond length of 3.6 Å.

IV. RESULTS AND DISCUSSION

A. Experimental determination of protein release rates from polymer nanoparticles

Using a single emulsion method, we formulated monodisperse PLGA NPs of size 85.3 nm, PLA NPs of size 102.5 nm, and PS-PLA NPs of size 160.3 nm, all with PDIs below 0.2 (Table I).

Due to the inability of accurately measuring BSA content in PS-PLA NPs because of absorbance/fluorescence interference from styrene π stacking,[34] we estimated that PS-PLA NPs contained the same initial BSA content as PLA NPs of

TABLE I. Nanoparticle characterization before and after BSA release experiments (n = 3 batches for all measurements).

Polymer type (MW in Da)	Mean diameter ± SEM (nm)	PDI ± SEM	Mean ZP ± SEM (mV)
PLGA (10–15 000)	85.3 ± 7.6	0.15 ± 0.01	−67.0 ± 2.2
PLA (10–15 000)	102.5 ± 4.9	0.15 ± 0.01	−62.1 ± 11.3
PS–PLA (5000:5000)	160.3 ± 21	0.11 ± 0.01	−38.2 ± 1.6

0.823 mg. We expect this approximation to be along the right magnitude or potentially higher than the actual value, considering the hydrophobic styrene groups would discourage greater BSA encapsulation. PLGA had an initial BSA content of 0.536 mg. We calculated the total amount of BSA released for PLA (0.286 mg BSA) to equal the difference between BSA content of PLA NPs before (0.823 mg BSA, 16.39% EE) and after release (0.537 mg BSA, 10.70% EE), and scaled the raw fluorescence of supernatant BSA values to this maximum release. We then scaled the raw fluorescence to corresponding BSA release concentrations for PLGA and PS-PLA. After a 7 day incubation period, PLGA, PLA, and PS-PLA achieved 8.12%, 34.74%, and 42.66% BSA release, respectively (Fig. 2).

PS-PLA had the greatest % BSA release and PLGA the least % BSA release after 7 days of incubation. Release is driven by water adsorption into and interaction with the polymer matrix that drives polymer dissolution.[35] Interestingly, PLA and PS-PLA exhibit a nearly identical release profile up to 3 days, then a greater rate of BSA release is seen in PS-PLA from 3 to 7 days. Experimentally, it is possible PS-PLA forms a PS core with a PLA outer layer, whereas PLA NPs are uniform in composition throughout the particle matrix. The initial pattern of release (up to 3 days) seen in PLA and PS-PLA suggests that BSA is evenly distributed among the PLA components of each formulation. However, BSA is not strongly associated with PS in the core of the PS-PLA NP, lending toward faster release from PS-PLA at later time points, as water adsorbs into the polymer core. These results would be further supported with future analysis of spatial distribution of BSA within the polymer NP matrix, and with precise determination of BSA content in PS-PLA NPs.

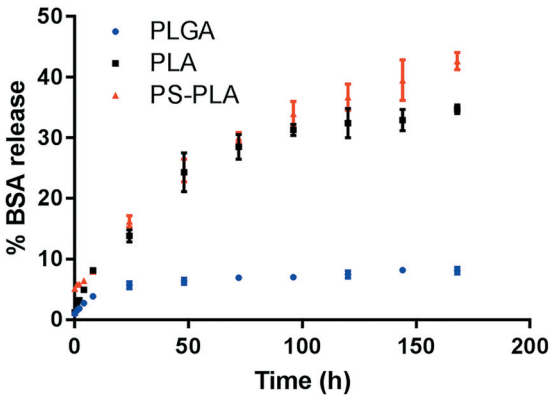

FIG. 2. Percent BSA release profile of BSA released against total BSA initially encapsulated for PLA (black), PS-PLA (red), and PLGA (blue) nanoparticles (n = 3 batches for all samples).

It is also important to note that transport-limited release is refuted given that there is no obvious correlation between nanoparticle size and % release. In fact, the qualitative correlation here is opposite of that expected in the context of diffusion limitations—the smallest particle has the slowest release. These observations suggest that computational modeling can provide useful insight into the role of nanoscale physical interactions in explaining differences in empirical protein release from chemically distinct NPs.

B. Aggregation tendencies of polymer surrogates

As demonstrated in Fig. 3(a), aggregation was observed in our MD simulations to occur relatively quickly between PS molecules in aqueous solution with either PS-PLA or PS alone, clearly driven by strong hydrophobic and aromatic interactions. Aggregation occurred more slowly in the solution with PS-PLA, where the presence of free PLA trimers

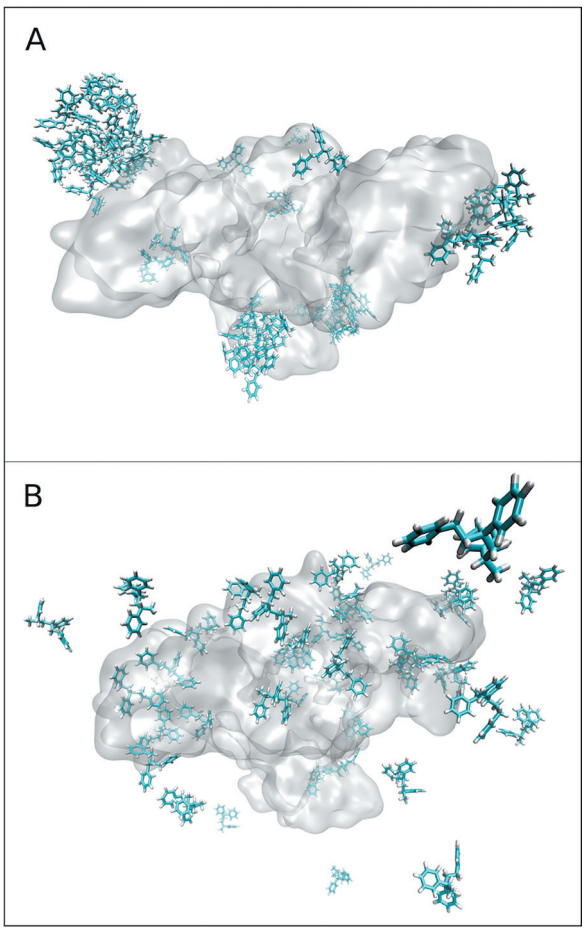

FIG. 3. Final snapshots from simulation trajectories of BSA in aqueous solutions with 2 wt. % PS, without (a) and with (b) restraints between PS atoms in neighboring molecules to prevent self-aggregation. BSA is shown in surface representation in transparent gray coloring to show PS binding to all sides of the surface. PS molecules are shown with carbon and hydrogen atoms colored cyan and white, respectively. Water and neutralizing counterions are not pictured.

could act to partially shield hydrophobic interactions between nearby PS molecules. After 50 ns, we concluded protein/PS interactions were no longer changing in the simulations due to significant PS aggregation. Based on our observations, PS self-interactions can out-compete interactions between the protein and PS surrogate molecules. We hypothesized this would manifest in faster release of BSA from PS-PLA particles than from PLGA or PLA NPs, that per our simulations should not suffer from polymer self-interactions and instead should have stronger overall binding with the encapsulated protein. This was verified by our experiments that, of the three NP formulations, PS-PLA showed the greatest % BSA release after 7 days of incubation (Fig. 2).

The high level of aggregation in our PS-based simulations prevented a detailed study of the molecular scale interactions between hydrophobic polymer substituents and protein surfaces. It is crucial to study these interactions because not all polymers with hydrophobic moieties will aggregate, as we demonstrate in Sec. IV E, which could provide new insight into protein release kinetics from polymer NPs. Furthermore, the possibility of preparing enzyme-nanoparticle formulations closer to the theta point of the polymer suggests the need to more carefully probe the specific protein/polymer interactions. To probe these interactions, we performed additional simulations of BSA in aqueous solutions with PS-PLA and PS alone with restraints in place to prevent aggregation between PS molecules (see Sec. III for details). As shown in Fig. 3(b), even after 200 ns of simulation, the PS remained completely dispersed in solution, leading to increased interactions between the protein and polymer surrogates, discussed in detail in Sec. IV C.

C. Amino acid binding preferences of polymer surrogates

To assess the amino acid binding preferences of the polymer surrogates, the fraction of contacts over the course of the MD trajectories was calculated between each polymer surrogate and the different types of amino acid residues on the surface of BSA. Fractional contacts were calculated by dividing the number of frames in which surface amino acid residues were in contact with a polymer surrogate by the total number of frames in the trajectory, and then summing over all residues of each type of amino acid. Contacts were defined between polymer surrogate molecules and protein surface residues within 4 Å of each other. The first 100 ns of each simulation trajectory was excluded to ensure the calculations were only performed over converged portions of the data. Figure S1 demonstrates that with few exceptions, the fraction of contacts with each amino acid type converged to within a few percent by approximately 100 ns with each polymer surrogate; extension of the simulation of BSA in the solution with PLGA to 500 ns further demonstrates that 100–200 ns is an appropriate timeframe over which to calculate fractional contacts of small polymer surrogates to protein surface residues (Fig. S2).[38] We also note that in quantifying binding trends, we did not consider BSA conformational changes in our calculations; the root mean squared deviation (RMSD) of the protein's Cα atoms from the crystal structure over the course of the simulations shows the structural integrity of BSA remained intact in all solutions, with similar fluctuations in the polymer surrogate solutions as in pure water (Fig. S3).[38]

The results for the fraction of surface amino acid types contacted by the polymer surrogates are shown in Fig. 4. The data have been normalized by the protein surface fraction of each amino acid residue type contacted by each polymer surrogate over the portion of the simulation trajectories from 100 to 200 ns, and error bars reflect the average standard deviation of calculations performed over four 25 ns portions in this timeframe. The results illustrate the specificity of protein/surrogate binding, in that the unique functional groups on the polymer surrogates lead to different amino acid binding preferences. The slightly more hydrophilic nature of PLGA is reflected in a small decrease in binding to hydrophobic residues and increase in binding to negatively charged residues compared to PLA; however, binding to most amino acids types is statistically indistinguishable for PLGA and PLA. Considering the earlier results of Fig. 2 that showed PLGA NPs had a significantly lower % BSA release compared to PLA NPs, we draw the conclusion that molecular scale interactions between the protein and surrounding host environment are of less importance than materials-level properties (e.g., polymer flexibility and hydration properties) in determining and controlling protein release kinetics from polymer NPs.

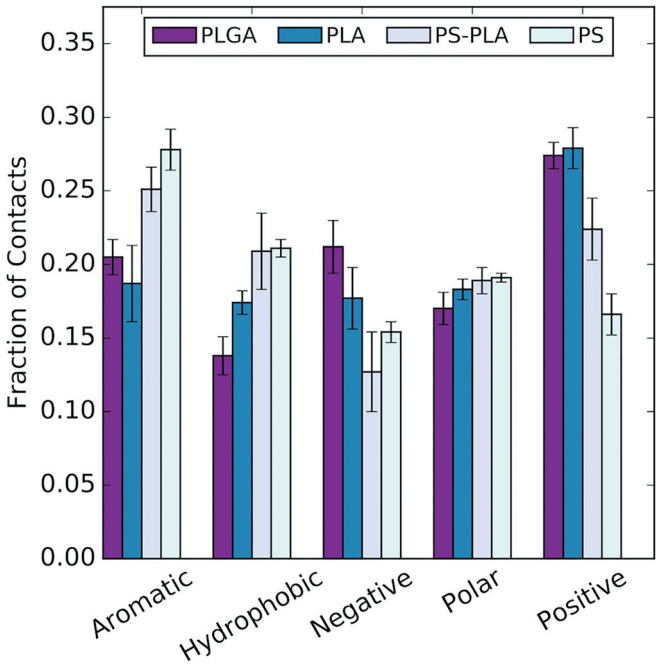

FIG. 4. Fraction of contacts to the different amino acid types on the surface of BSA by polymer surrogates. Error bars represent the average standard deviation of calculations performed on consecutive 25 ns portions over the second half of each 200 ns simulation trajectory (i.e., sample size of n = 4).

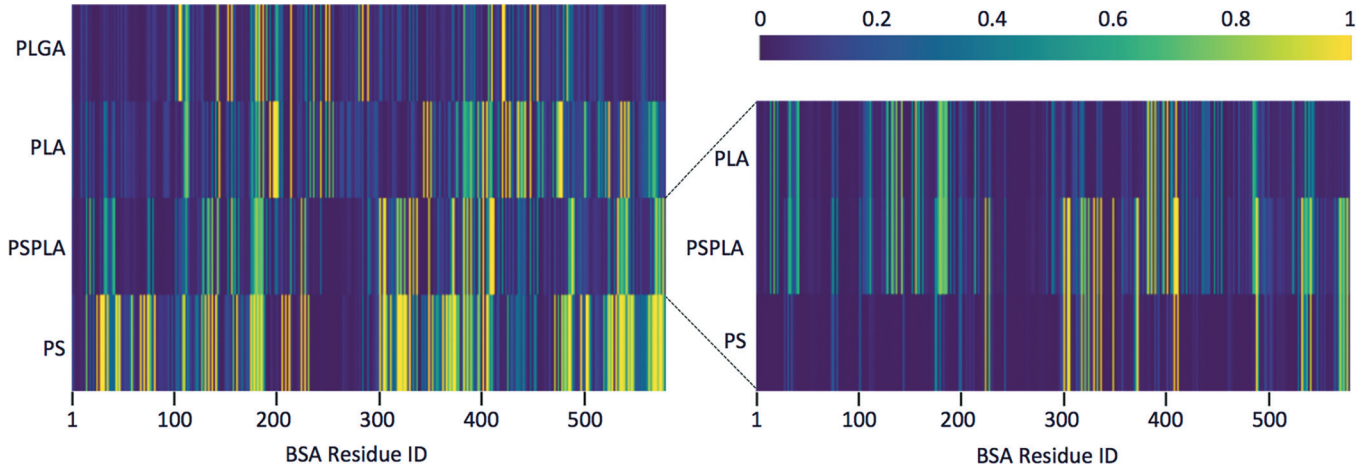

FIG. 5. Occupancy heat maps for BSA residues: (left) BSA residue occupancy for PLGA, PLA, PS-PLA, and PS simulations. PS simulations include a coordination potential to discourage aggregation. Occupancy was calculated as the fraction of surrogate contacts for each residue over the last 100 ns; (right) PLA, PS-PLA, and PS occupancy from the PS-PLA simulation.

Comparing the results in Fig. 4 for the PS-PLA solution versus the solutions with PLGA or PLA shows very different binding behavior for PS-PLA. Whereas PLGA and PLA are seen to bind more frequently to surface residues through strong electrostatic interactions (i.e., to both negatively and positively charged residues), PS-PLA binds more frequently to hydrophobic and aromatic residues. These trends are intuitive due to the predominantly hydrophilic nature of PLGA and PLA, and the partially hydrophobic nature of benzene-containing PS-PLA. Comparing instead the results for PS-PLA with either PLA or PS alone shows the fraction of BSA surface contacts targeted by PS-PLA falls in between that of PLA and PS for nearly every amino acid type. This finding implies that binding can be modulated by altering the relative surrogate compositions, supporting the notion that changes in the NP functionality will lead to differential protein binding and controlled protein release rates from NPs formulated using these polymers. Future experimental studies are planned to explore the validity of this hypothesis. Figure 4 shows that the fractional occupancy values for PS-PLA tend to be slightly closer to the values for PS over PLA, despite the approximately 25%/75% molar ratio of PS to PLA in the solution. Therefore, we infer that the nature of the relationship between the composition of the NP substituents and the resultant characteristics of protein/polymer binding is nonlinear and complex, and may follow a "winner takes all" approach, as we investigate in Sec. IV D. Additionally, while the results of Fig. 4 tell us the frequency of protein/polymer surrogate binding, they do not tell us the relative strength of binding of the different polymer surrogates to protein surface residues, which will also be addressed in Sec. IV D.

D. Spatiotemporal resolution of binding of polymer surrogates to protein surface residues

It is necessary to further explore the spatiotemporal binding characteristics of each polymer on the BSA surface to confirm or rule out the central importance of polymer–protein interactions for controlled release. Differences in protein surface coverage and/or polymer residence times could provide the necessary explanation for differences in experimentally observed release times. For each MD trajectory, the fractional occupancy of each BSA residue was calculated, followed by the generation of occupancy heat maps to illustrate the spatial distribution of binding. Occupancy heat maps were created in Python 2.7 (Ref. 36) from the preprocessed MD trajectory data, and the fractional occupancy was calculated for each residue by dividing the number of frames contacting a polymer substituent by the total number of frames (50 frames per 1 ns). Average polymer residence times for each residue were calculated with an in-house Python script analyzing the same preprocessed data. We also tracked highly occupied residues and trimers with high residence time in VMD (Ref. 37) to resolve inconsistencies between isolated PS/PLA molecules and mixed binding in PS-PLA. Figure 5 includes heat maps for each independent polymer simulation as well as a componentwise breakdown of occupancy in the PS-PLA simulation.

Although PLGA and PLA have similar amino acid type binding preferences (Fig. 4), the occupancy heat maps suggest the spatial distribution of their binding is different (Fig. 5, top left). The high-occupancy band from H285 to E291 is unique to PLGA, whereas the thick band from V421 to Y449 is present only for PLA. Overall, the surface coverage for PLA and PLGA is similar, especially compared to the prolific binding of PS in the coordination-constrained simulation. Table II includes average occupancy per BSA residue for each simulation. The average occupancy is similarly

TABLE II. Trimer mean occupancy per BSA residue.

Polymer type	Mean occupancy ± Std dev
PLGA	0.16 ± 0.021
PLA	0.23 ± 0.005
PS-PLA	0.23 ± 0.016
PS	0.38 ± 0.031

nondiscriminatory for PLGA and PLA, predicting more surface binding for PLA than PLGA. The slight differences in physical interactions do not appear to capture the differences in experimental binding.

The occupancy results above also provide useful information regarding the experimental hypothesis that PS-PLA forms a core–shell particle. With the added coordination potential to prevent aggregation, PS binds persistently to the majority of BSA surface residues. Without the coordination potential, PS aggregates and interacts sparingly with the protein (Fig. S4).[38] Thus, while PS has a strong preference for the protein over water, it has a much higher affinity for self-interaction. The PS-PLA simulation with PS interaction constraints (represented by the right side of Fig. 5) exhibits a winner take all behavior, where only the polymer substituent with the greatest affinity for a given residue binds to that residue. The PS-PLA simulation without the coordination constraint on PS is more representative of the experimental hypothesis, where PS aggregates and the binding characteristics are dominated by PLA. It may be necessary to use a random copolymer instead of a block copolymer such as PS-PLA to tune aggregation and protein/polymer surrogate binding. Section IV E includes an extension of this computational approach to such a polymer.

E. Tuning polymer self-interactions

Building on our finding that the self-aggregation tendencies of the polymer surrogates may play an important role in determining protein release kinetics, we performed MD simulations of BSA in solution with a polymer surrogate that we hypothesize would allow for more control over the protein encapsulation process. Figure 6 shows the structure of this new polymer surrogate, PSAC, which we simulated as trimers of alternating PS and acrylate monomers (six units total per molecule) to mimic experimental conditions of a PSAC random copolymer with an approximately 50%/50% molar ratio of PS and acrylate. Like PS-PLA, PSAC has strong hydrophobic moieties, though in contrast to PS-PLA, PSAC has no tendency to self-aggregate in solution at the intercellular *p*H of the brain (∼7.2), as determined in our MD simulations. Figure 6 shows that even after the full 200 ns of simulation time, the PSAC molecules are fully distributed around the protein surface, indicating protein/PSAC interactions can outcompete PSAC-PSAC interactions. The difference in aggregation tendencies of the polymer surrogates observed in our simulations is likely due to the different ways in which the monomers are joined in each polymer surrogate chain (i.e., as separate trimers in PS-PLA and as alternating monomers in PSAC). In PSAC, PS-PS interactions were largely inhibited by the unavoidable presence of the neighboring, hydrophilic acrylate monomers.

Figure 7 shows the fraction of amino acid types on the surface of BSA contacted by PSAC compared to PS-PLA and PLGA, where the data and error bars have been calculated and treated as described earlier. Like with previously studied systems, Fig. S5 shows the fraction of contacts with

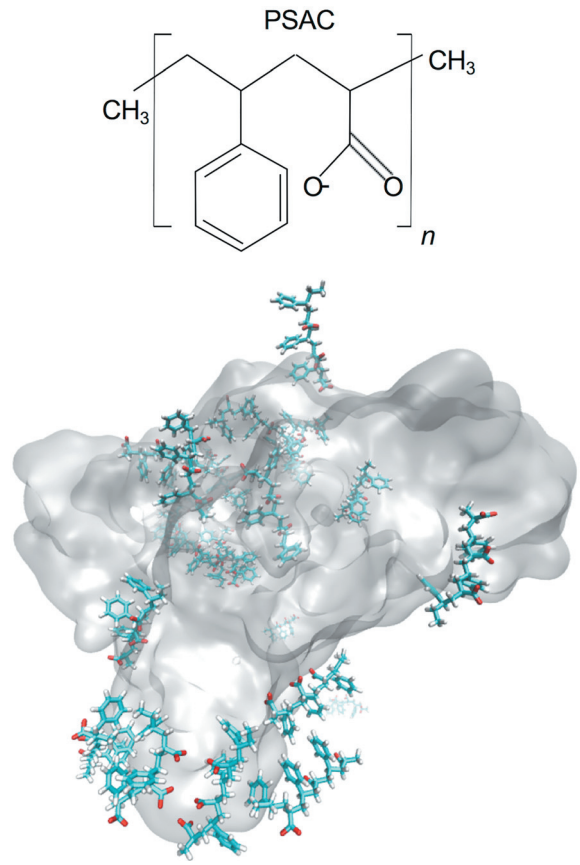

FIG. 6. Top: Representative structure of PSAC copolymer. Bottom: Snapshot from the end of a 200 ns simulation trajectory of BSA in an aqueous solution with 2 wt. % PSAC, with no restraints to discourage PSAC self-aggregation.

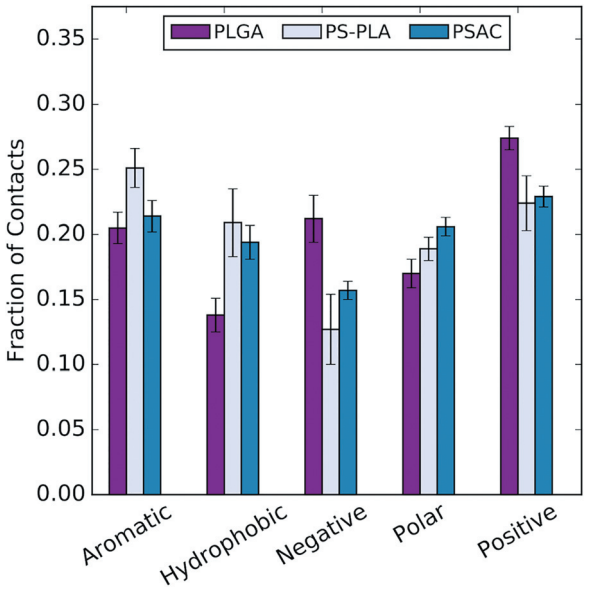

FIG. 7. Fraction of contacts for different amino acid types on the surface of BSA in an aqueous solution with PSAC compared to with PS-PLA or PLGA. Error bars represent the average standard deviation of calculations performed on consecutive 25 ns portions over the second half of each 200 ns simulation trajectory (i.e., sample size of n = 4).

each amino acid type converges in approximately 100 ns for the simulation of BSA in the solution with PSAC. Additionally, Fig. S6 shows the structure of BSA remains stable throughout the 200 ns simulation in the solution with PSAC.[38] The results of Fig. 7 show the binding characteristics of PSAC are similar to PS-PLA when compared to PLGA, in that PSAC binds more often to hydrophobic and aromatic residues and less often to positive and negatively charged residues than does PLGA. However, the magnitude of the changes in binding to the different amino acids types between PSAC and PLGA is generally smaller than between PS-PLA and PLGA, which arise from the separately simulated trimers of PS and PLA in PS-PLA that results in more definitive binding to specific amino acid types. These findings highlight the sensitivity of our approach to both the individual chemical functionalities in a given polymer, as well as the overall polymer chemistry that is driven by the spatial proximity of individual functional groups in the polymer chain. Based on our observations, we would expect slower protein release rates from PSAC NPs compared to PS-PLA NPs due to decreased polymer self-interactions leading to increased protein/polymer interactions. However, we still anticipate PSAC NPs would lead to faster release compared to PLGA or PLA NPs due to weaker overall binding with the largely hydrophilic BSA protein.

At a neutral *p*H of 7.2, acrylate side chains in PSAC molecules would be almost completely deprotonated, as they were in our simulations. Interestingly, additional simulations we ran with protonated acrylate side chains showed rapid aggregation of PSAC molecules around the surface of BSA (Fig. S7).[38] This finding highlights that a small change in the chemical functionality of the NP could dramatically shift the balance of polymer self-interactions versus protein/polymer interactions, thereby affecting protein release rates. As previously hypothesized, some NPs such as those made with PS-PLA copolymers may form a tight core with polymer that is not exposed to physiological conditions. Thus, changes in NP formulation methods may lead to tunable core properties to control the degree of aggregation and thus protein release kinetics.

F. Effect of surrogate length on binding convergence and characteristics

By exploring the preference of polymer surrogates of varying lengths for specific amino acid types on the protein surface, we can assess the validity of using small polymer molecules as proxies for more realistic systems. To stringently test this idea, we performed additional MD simulations of BSA in aqueous solutions with 2 wt. % of the monomeric forms of hydrophilic PLGA (LGA) and hydrophobic PSAC (SAC). Figure S8 shows the RMSD of the Cα atoms from the crystal structure of BSA in these new solutions is very similar to the RMSD values in solutions with the trimeric forms of these NP substituents (i.e., PLGA and PSAC, respectively), discussed in Secs. IV C, IV D, and IV E of the manuscript.[38] A comparison of the fraction of amino acid types on the surface of BSA contacted by the monomeric and trimeric polymer surrogates is shown in Fig. 8, and Fig. S9 shows these contacts converge in similar timeframes for the monomeric and trimeric polymer surrogates (~75–100 ns).[38] The results of Fig. 8 indicate that in general, the binding characteristics of monomeric LGA and SAC closely match those of trimeric PLGA and PSAC, respectively, for all five amino acid types on the surface of BSA. For example, the amino acids to which the surrogates bind most strongly and weakly are the same for each monomer/trimer pair: LGA/PLGA bind most strongly to positively charged residues and most weakly to hydrophobic residues, and SAC/PSAC bind most strongly to positively charged residues and most weakly to negatively charged residues. Interestingly, Fig. 8 shows similar binding to aromatic residues for both the hydrophilic and hydrophobic polymer surrogates. This is likely due to the close proximity of the benzene ring and carboxylate ion on the SAC/PSAC backbone that limits the frequency and strength of aromatic interactions with surface residues. This was discussed earlier as the main reason for why PSAC does not aggregate in solution like PS-PLA with similar hydrophobic moieties. Overall, these findings suggest that qualitatively, the use of small polymer surrogates, even with the greatest simplification of simulating long-chained polymers as monomeric units, can be used to decipher and predict governing principles of protein/polymer interactions.

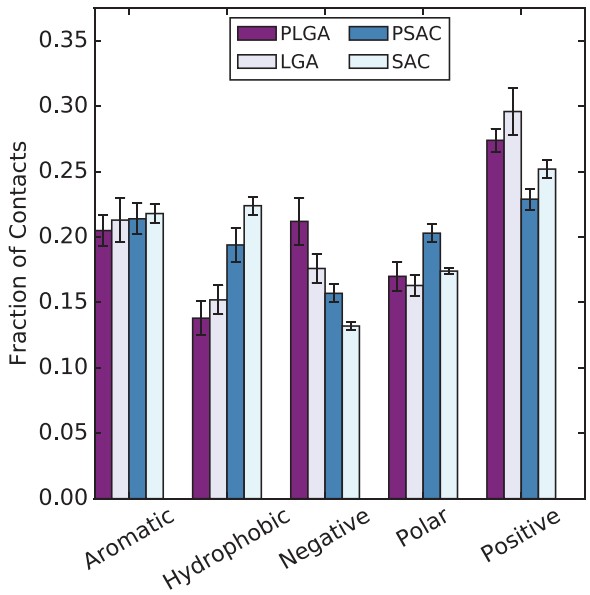

FIG. 8. Fraction of contacts for different amino acid types on the surface of BSA in solutions with monomeric or trimeric LGA or PLGA copolymer, or SAC or PSAC copolymer, respectively. Error bars represent the average standard deviation of calculations performed on consecutive 25 ns portions over the second half of each 200 ns simulation trajectory (i.e., sample size of n = 4).

V. SUMMARY AND CONCLUSIONS

In this work, we demonstrate a combined experimental and computational approach to gain insight into the driving forces of protein release from polymeric nanoparticles. This

approach provides a holistic picture of BSA release from NPs by describing physical interactions with macroscopic and microscopic detail.

Experimental results suggest transport limitations do not significantly restrict protein diffusion from larger NPs. The similarity between measured BSA release rates from PLA and PS-PLA NPs, and support from MD simulations, imply the diblock copolymer PS-PLA assumes a core–shell structure. The simplified system emphasizes the importance of physical interactions between a protein and trimeric polymer surrogates and selectively ignores polymer conformation and transport limitations to protein release. Although rapid screening of physical interactions between polymer constituents and a target protein is computationally tractable, it is unlikely that these physical interactions are sufficient descriptors for protein retention in the complex NP environment. The relative affinity of a polymer for self-interaction over protein interaction seems to be an important factor in release. PS aggregates in normal MD solutions, corresponding to exclusion or rapid clearance of protein in practice. A more complete model of the microscopic environment is difficult to clearly define, but is perhaps necessary for an accurate description of the atomic scale interactions of encapsulated proteins.

Spatial binding resolution for protein–nanoparticle systems is of interest for a wide range of biomedical applications. Beyond controlled release, the potential for design of synthetic particles that specifically interact in biological signaling and protein interaction pathways depends on the precision with which we can target protein surface patches. This work demonstrates the feasibility of progressing from chemical intuition to experimental and computational observation of specific protein–biomaterial interactions.

ACKNOWLEDGMENTS

J.P., J.S., and K.G.S. acknowledge the support from NSF Award No. CBET-1264459. E.A.N. acknowledges support from the Burroughs Wellcome Fund (BWF) Career Award at Scientific Interfaces. This work was facilitated though the use of advanced computational, storage, and networking infrastructure provided by the Hyak supercomputer system and funded by the STF at the University of Washington.

[1]A. J. Sawyer and T. R. Kyriakides, Adv. Drug Delivery Rev. **97**, 56 (2016).
[2]S. Cohen, T. Yoshioka, M. Lucarelli, L. H. Hwang, and R. Langer, Pharm. Res. **8**, 713 (1991).
[3]D. Peer, J. M. Karp, S. Hong, O. C. Farokhzad, R. Margalit, and R. Langer, Nat. Nanotechnol. **2**, 751 (2007).
[4]C. M. Moore, N. L. Akers, A. D. Hill, Z. C. Johnson, and S. D. Minteer, Biomacromolecules **5**, 1241 (2004).
[5]M. J. González-Guerrero, F. J. del Campo, J. P. Esquivel, F. Giroud, S. D. Minteer, and N. Sabaté, J. Power Sources **326**, 410 (2016).
[6]Y. Liu *et al.*, Nat. Nano. **8**, 187 (2013).
[7]B. L. Montalvo-Ortiz, B. Sosa, and K. Griebenow, AAPS PharmSciTech **13**, 632 (2012).
[8]G. Srinivas, D. E. Discher, and M. L. Klein, Nat. Mater. **3**, 638 (2004).
[9]H. Fukunaga, J. Takimoto, and M. Doi, J. Chem. Phys. **116**, 8183 (2002).
[10]S. Samanta and D. Roccatano, J. Phys. Chem. B **117**, 3250 (2013).
[11]S. Ahmad, B. F. Johnston, S. P. Mackay, A. G. Schatzlein, P. Gellert, D. Sengupta, and I. F. Uchegbu, J. R. Soc. Interface **7**, S423 (2010).
[12]S. M. Loverde, V. Ortiz, R. D. Kamien, M. L. Klein, and D. E. Discher, Soft Matter **6**, 1419 (2010).
[13]E. Moeendarbary, T. Y. Ng, and M. Zangeneh, Int. J. Appl. Mech. **2**, 161 (2010).
[14]V. Ortiz, S. O. Nielsen, D. E. Discher, M. L. Klein, R. Lipowsky, and J. Shillcock, J. Phys. Chem. B **109**, 17708 (2005).
[15]M. F. Zambaux, F. Bonneaux, R. Gref, P. Maincent, E. Dellacherie, M. J. Alonso, P. Labrude, and C. Vigneron, J. Controlled Release **50**, 31 (1998).
[16]L. Martinez, R. Andrade, E. G. Birgin, and J. M. Martinez, J. Comput. Chem. **30**, 2157 (2009).
[17]J. Wang, R. M. Wolf, J. W. Caldwell, P. A. Kollman, and D. A. Case, J. Comput. Chem. **25**, 1157 (2004).
[18]M. J. Frisch *et al.*, *Gaussian 09* (Gaussian, Inc., Wallingford, CT, 2009).
[19]W. D. Cornell, P. Cieplak, C. I. Bayly, and P. A. Kollman, J. Am. Chem. Soc. **115**, 9620 (1993).
[20]J. A. Maier, C. Martinez, K. Kasavajhala, L. Wickstrom, K. E. Hauser, and C. Simmerling, J. Chem. Theory Comput. **11**, 3696 (2015).
[21]W. L. Jorgensen, J. Chandrasekhar, J. D. Madura, R. W. Impey, and M. L. Klein, J. Chem. Phys. **79**, 926 (1983).
[22]J. R. Casey, S. Grinstein, and J. Orlowski, Nat. Rev. Mol. Cell Biol. **11**, 50 (2010).
[23]C. Curtis, M. Zhang, R. Liao, T. Wood, and E. Nance, Wiley Interdiscip. Rev. Nanomed. Nanobiotechnol. **9**, e1422 (2017).
[24]E. Nance, C. Zhang, T. Y. Shih, Q. Xu, B. S. Schuster, and J. Hanes, ACS Nano **8**, 10655 (2014).
[25]E. Nance, F. Zhang, M. K. Mishra, Z. Zhang, S. P. Kambhampati, R. M. Kannan, and S. Kannan, Biomaterials **101**, 96 (2016).
[26]E. A. Nance, G. F. Woodworth, K. A. Sailor, T. Y. Shih, Q. Xu, G. Swaminathan, D. Xiang, C. Eberhart, and J. Hanes, Sci. Transl. Med. **4**, 149ra119 (2012).
[27]M. J. Abraham, T. Murtola, R. Schulz, S. Páll, J. C. Smith, B. Hess, and E. Lindahl, SoftwareX **1–2**, 19 (2015).
[28]B. Hess, H. Bekker, H. J. C. Berendsen, and J. G. E. M. Fraaije, J. Comput. Chem. **18**, 1463 (1997).
[29]U. Essmann, L. Perera, M. L. Berkowitz, T. Darden, H. Lee, and L. G. Pedersen, J. Chem. Phys. **103**, 8577 (1995).
[30]G. Bussi, D. Donadio, and M. Parrinello, J. Chem. Phys. **126**, 014101 (2007).
[31]H. J. C. Berendsen, J. P. M. Postma, W. F. Vangunsteren, A. Dinola, and J. R. Haak, J. Chem. Phys. **81**, 3684 (1984).
[32]M. Parrinello and A. Rahman, J. Appl. Phys. **52**, 7182 (1981).
[33]G. A. Tribello, M. Bonomi, D. Branduardi, C. Camilloni, and G. Bussi, Comput. Phys. Commun. **185**, 604 (2014).
[34]A. Kuo, CheM **1**, 80 (2011).
[35]W. B. Liechty, D. R. Kryscio, B. V. Slaughter, and N. A. Peppas, Annu. Rev. Chem. Biomol. Eng. **1**, 149 (2010).
[36]G. Van Rossum, "Python programming language," in *USENIX Annual Technical Conference* (2007), p. 36.
[37]W. Humphrey, A. Dalke, and K. Schulten, J. Mol. Graphics **14**, 33 (1996).
[38]See supplementary material at http://dx.doi.org/10.1116/1.4983154 for convergence plots, protein conformational analysis, and comparison of polystyrene simulations with and without coordination bias.